IJSES
Volume 6, Issue 2, pp. 94-106, 2022.
International Journal of Scientific Engineering and Science
ISSN (Online): 2456-7361

# Seismic Performance of Tubular Square Column to Stiffened I-Beam

Mohamed G. Abdolwahab[1], Ahmed H. Yousef [2], Ehab H. Ahmed[3]
[1]Research Student, Structural Engineering Department, Faculty of Engineering, Ain Shams University, Cairo, Egypt
Assistant Lecturer, Construction Engineering Department., Faculty of Engineering, Egyptian Russian University, Cairo, Egypt
[2]Professor of Steel Structures and Bridges, Structural Engineering Department, Faculty of Engineering, Ain Shams University, Cairo, Egypt
[3]Professor of metallic constructions, Structures and metallic constructions Research Institute Housing and Building, National Research Center

***Abstract*—** *This paper investigates the behaviour of welded steel I-beams to hollow square tubular columns. Six finite element stiffened models of welded steel connections, with the same designs, are exposed to cyclic loads and verified against the experimental results of unstiffened model obtained from previous researches and current design guides. During the testing, the connections' flexibility and strength are assessed, and damage phenomena and failure modes are investigated. The connection damage is discovered to be a cumulative fracture process that leads to significant gradual degradation of the connection's mechanical capabilities. Quantificational analyses of cyclic loading induced damage are also carried out in order to investigate the level of connection damage based on different loading intensities. A numerical investigation of finite element modelling is also carried out to validate the experimental results, and a satisfactory agreement is obtained. The test results and FE modelling give benchmark data for unstiffened and stiffened welded connections, where the results show that using proper stiffener configuration affects the stress distribution through the connection and increases the ultimate moment of the connections.*

***Keywords*—** *Seismic Performance, Welded connection, Square column, Box section, Finite element analysis, Stiffener configurations, Ultimate strength, Moment connections.*

## I. INTRODUCTION

In comparison to H-shaped columns, box-columns have more rigidity and torsional strength. These columns can also withstand fire better than H-shaped columns because they have a larger cross-sectional area and can take use of flame-resistant fibers. Because reinforced concrete-filled box-columns have good axial strength, they are widely used in buildings that require higher axial strength and have adequate seismic performance when subjected to cyclic loading. The features of box-columns have made them excellent for steel moment frames, and their seismic performance has recently caught the interest of researchers.

In general, the results of experiments and numerical analyses on both box and H-shaped columns showed that the transfer of moment from the connection to the box-column is less than that to the H-shaped column. This behavior in moment transfer can be attributed to the out-of-plane deformation of flanges in the box-column [1]. Next, the studies of Saneei Nia et al. [2-5] are addressed who examined the I-beam to box-column connections experimentally and numerically. In their study, by performing six full-scale tests on WUF-W moment connections, they concluded that the plastic hinge was generated in the beam's predicted area near the connection. Nevertheless, the damage and deterioration did not occur in the columns, panel zones, continuity plates, web shear plates, and the beam web and flange connection to the column at the point of penetration welds. In all the tested samples, a minimum of 0.04 rad inter-story drift was observed without strength degradation, and of a 0.06 rad inter-story drift was occurred with less than 20% strength degradation. Also, two full-scale tests were performed for direct connection of beam with increased cross-section, in which the web shear plate was removed. The plastic hinge was directed away from the column face by increasing the beam's cross-section near the connection. The results indicated that their connection could be classified as a moment connection to a box-column in a special moment frame by providing the required inelastic rotation capacity.

Song et al. [6] & [7] investigated the behavior of double-angle bolted and unstiffened welded connections in square and tubular columns subjected to monotonic and cyclic loading following the SAC loading protocol. In this study, they argued that although the double-angle bolted connections are designed based on resistance to shear loads, the double-angle connections reduce damage subjected to cyclic loading. The column panel thickness at the panel zone significantly affects the rotation of the connection and stress distribution near the column base plate. The damage to the components depends on the total deformation range; it seems quite normal that the connections show different behaviors subjected to monotonic and cyclic loading. Since the failure mode generally depends on the weakest component in the element, failure modes were observed at the bolts and welds of angles on the beam web for double-bolted connections, while failure modes were reported at the tensile flanges and the panel zone for unstiffened welded connections.

Recently, steel tube has drawn a widespread interest as column members of steel structures. While many advantages exist, their use in building construction has been limited due to the lack of construction experience and the complexity of connection detailing. These components have yet to be investigated to bring about their full potential with respect to their applications.

International Journal of Scientific Engineering and Science
Volume 6, Issue 2, pp. 94-106, 2022. ISSN (Online): 2456-7361

Several upgrading strategies can be applied in the connection, such as using different column cross section shapes with various stiffener configurations. Regarding the connections of steel tube, the most convenient connection is to attach the steel I-beam through an external stiffener. This is an efficient method. The stiffener reduces the stress concentration at the column steel wall preventing it from failure. Therefore, recent investigations have focused on the development of various shapes of stiffeners. Numerous research works [8 - 15] have recently been carried out studying the variation of ultimate moment of the connections between steel I-beams and steel tube columns.

The purpose of this study is to demonstrate the effect of stiffener configurations on the ultimate moment of the connections between steel I-beams and steel tube column. A parametric study is carried out taking into consideration stiffener shapes. The analytical investigation utilizes nonlinear finite element modeling techniques using ANSYS program [16].

## II. Experimental Model

### *2.1. Specimens and fabrication*

The unstiffened welded connections were made of I-beams and tubular columns through fillet welds, as shown in Fig. 1. The I-beams were IPE 300. The square tubular columns, with the cross section of 250 x 250 mm. The column wall thickness was used equal to 10 mm. Additionally, plates with nominal thickness of 20 mm were welded on the top and bottom of the column, whilst two stiffeners were welded to the I-beam, 1400 mm away from the column surface, where the load was applied. The average size of the fillet welds between the I-beam and the tubular column wall was measured as 6 mm and 10 mm for vertical and horizontal weld, respectively. According to AISC [17], the columns, beams, and stiffeners are compact sections. The yield strength of the fabricated sample is, 350 MPa for columns, 300 MPa for all stiffeners, and lastly 280 MPa for beams, according to the test results, with the modulus of elasticity of steel, Es, being 200000 MPa.

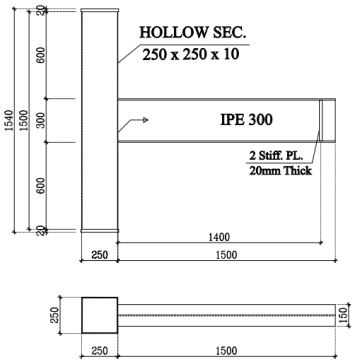


Fig. 1. Schematic Drawing of Experimental Specimen (Unstiffened welded connections)

### *2.2. Setup and loading protocol*

The loading setup and boundary conditions for the cyclic loading tests are as shown in Fig. 2. The column was set with hinged supports at 180 mm from its ends, while the degrees of freedom Ux and Uy of the column top ends were restrained except the axial movement Uz was valid. The column's boundary conditions were carefully chosen to limit the effect of the column's overall deformation. A constant axial load of 300 kN was exerted on the top of the column during the test. The cantilever I-beam was loaded with cyclic actuator with 900 kN tension and compression loading capacity. The actuator was vertically connected to the beam through a uniform joint and used to exert a displacement-controlled load. It is worth noting that compressing the beam toward ground (downward direction) is taken as negative loading direction. The cyclic loading test was carried out according to the ANSI/AISC SSPEC-2002 [18] cyclic loading protocol, as shown in Fig. 3. When the major load drop occurred or the actuator reached its max. capacity, the test was stopped.

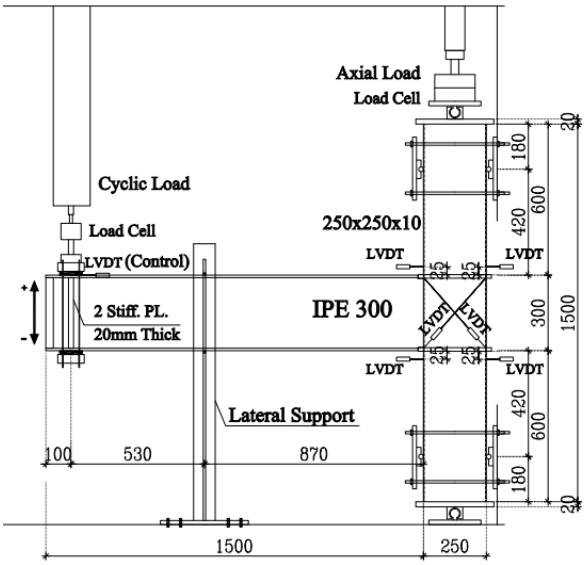


Fig. 2. Test setup and Loading system (All Dim. in mm)

International Journal of Scientific Engineering and Science
Volume 6, Issue 2, pp. 94-106, 2022. ISSN (Online): 2456-7361

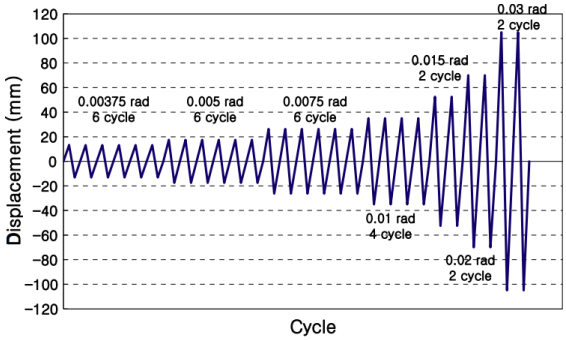


Fig. 3. Cyclic loading protocol (ANSI/AISC SSPEC-2002.).

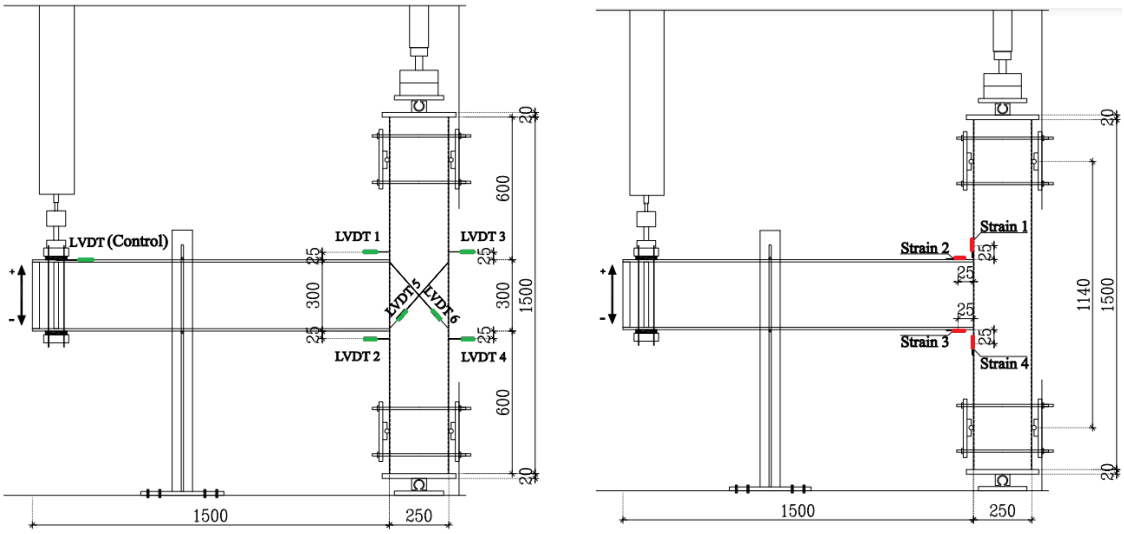


(a) Displacement gauges (b) strain gauges

Fig. 4. Arrangement of displacement gauges and strain gauges located at the center line of the beam column connection. (Dim. in mm)

### *2.3. Instrumentation*

In order to interpret the experimental behaviour, various data such as load versus displacement relationship, deformation of different components and strain values were measured using displacement and strain gauges. The arrangement of displacement gauges is shown in Fig. 4(a), while the arrangement of strain gauges is depicted in Fig. 4(b). Displacement gauges and strain gauges located at the axis of symmetry of the beam–column connection. All of the data is immediately entered into the computer, and curves are displayed automatically.

## III. NUMERICAL ANALYSIS

A three-dimensional finite element model has been created to allow a wide parametric investigation of the behaviour of moment connections between steel I-beams and square tube columns. Nonlinearities of both material and geometric nature are taken into account. All elements are defined as an individual bodies in the ANSYS programme [19] for the steel tube, steel beams, column stiffener, and end plates, as shown in Fig. 2. The finite element model details are described in the following subsections.

### *3.1. Modelling of steel parts*

Solid element SOLID45 is used to model the steel parts. It has membrane and bending capabilities and has eight nodes with three transitional degrees of freedom at each node; three translations and three rotations. At both ends, the columns are connected to thick end plates to distribute the load and reduce stress concentration.

### *3.2. Material properties*

Material properties of the column steel wall, stiffener plates and steel beam are defined by the tensile test results of coupons taken from specimens. Yield stress, shear modulus, and Poisson's ratio of the end column plates are as those of the steel solid element but with higher modulus of elasticity to avoid the deformations of the plates. The steel parts are defined by bilinear stress strain curve as shown in Fig. 5. Initial elastic modulus of elasticity is 200 kN/mm$^2$ and the tangential modulus of elasticity is defined as 0.01 of the elastic modulus. Steel grade 52 is used with specified yield stress equal to 360 N/mm$^2$. Shear modulus is taken 81 kN/mm$^2$ and Poisson's ratio is assumed to be 0.3. Yield stress, shear modulus and Poisson's ratio of the end column plates are as those of the steel solid element but with higher modulus of elasticity to distribute the load and reduce stress concentration.

International Journal of Scientific Engineering and Science
Volume 6, Issue 2, pp. 94-106, 2022. ISSN (Online): 2456-7361

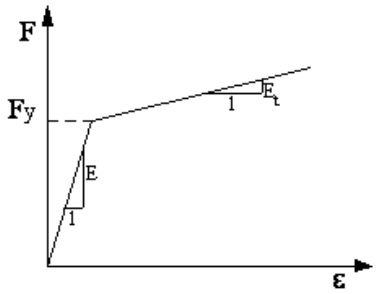


Fig. 5. Bilinear stress strain curve for steel

*3.3. Loads, boundary conditions and nonlinear analysis*

A distributed pressure is applied at the surface of the column upper end plate. An initial imperfection, of (1/1000) times the length of the column is considered. The end surfaces of the tube column are restrained while ends of steel I-beams are free in which vertical stiffener plates are used and applied with a cyclic loading test that carried out according to the ANSI/AISC SSPEC-2002 [18] cyclic loading protocol, as shown in Fig. 3. At 180 mm from the ends of the steel column, are modelled with all two translation degrees of freedom restrained $U_x$ and $U_z$ except for the longitudinal direction of steel column $U_y$, as well as the rotational degree of freedom, $R_x$, about the beam longitudinal axis. The "Newton-Raphson" approach is employed to solve geometric nonlinearity. The results are accurately estimated by incremental steps until failure occurs. Solution technique is the arc length method. No weld failure is studied, so common nodes for the steel beam and the steel column tube at the weld locations or for stiffener and steel I-beam flange are provided.

## IV. Comparison Between Experimental and Analytical Results

The results obtained from the finite element analysis are verified against the experimental results of the unstiffened beam-column joint. These tests show the ultimate moment of the connection between steel I-beam, of IPE 300, and square tube column, of 250 x 10, under the effect of in-plane bending moment due to cyclic load. The beam flange is welded to the column with 10 mm fillet weld; meanwhile the beam web is welded to the column on both sides of the web with 6 mm fillet welds. The length of the column is 1500 mm, as well as the length of the beam. Column is loaded axially with 300 kN while beam end are applied with a cyclic load. The moment is obtained by multiplying the force at beam support by the distance between the support and the center of the column. The tables and curves show that the results are in good correlation with the experimental results and proven to simulate the behavior of the connection effectively.

Table 1, Figs. 6 and 7 shows the ultimate moment of the connection of finite element analysis, $M_{(FEM)}$ and experimental results, $M_{(TEST)}$. Fair agreement is achieved between both experimental and analytical results for most specimens. As expected, the analytical model shows result higher than the experimental, due to the perfect conditions assumed for the finite element model, for example, the effect of weld and residual stresses are not included. Figs. 8 and 9 shows the deflection versus applied cyclic load relationship as hysteresis loops and envelop curve, respectively for both finite element model and experimental results. Similarly, Figs. 10 and 11 illustrates the stiffness degradation and the energy dissipation, respectively. It can be noticed that the two curves for every figure are almost identical with good agreement.

Table 2 shows the maximum load values at each cycle of the cyclic load protocol for both the experimental sample, **$P_{(TEST)}$** and the analytical model, **$P_{(FEM)}$**. The standard deviation of the ratio between the loads at each step equal to 0.03. This demonstrates the theoretical model's accuracy as well as its applicability to the parametric study work.

TABLE 1. Ultimate strength of experimental and analytical moment connection

| **Unstiffened Sample (Id)** | **B.C. TEST** | **B.C. FEM** | **Diff. between TEST and FEM** |
|---|---|---|---|
| **Ultimate Moment value** | $M_{ult\ (TEST)}$ (kN.m) | $M_{ult\ (FEM)}$ (kN.m) | $M_{ult\ (FEM)}/M_{ult\ (TEST)}$ |
| | 88.8 | 93.9 | 1.05 |

TABLE 2. The major test results of experimental and analytical moment connection

| **Δ (mm)** | **B.C. TEST** | **B.C. FEM** | **$P_{(TEST)}/P_{(FEM)}$** |
|---|---|---|---|
| | **P (kN)** | **P (kN)** | |
| 120 | 54.35 | 54.50 | 0.99 |
| 105 | 57.73 | 53.34 | 1.08 |
| 90 | 55.61 | 53.84 | 1.03 |
| 75 | 58.28 | 54.15 | 1.07 |
| 60 | 54.71 | 53.21 | 1.02 |
| 45 | 50.34 | 51.20 | 0.98 |
| 30 | 42.46 | 47.24 | 0.9 |
| 23 | 37.04 | 43.47 | 0.85 |
| 15 | 30.86 | 35.54 | 0.87 |
| 11 | 25.1 | 29.07 | 0.87 |
| 8 | 19.6 | 22.65 | 0.87 |
| 6 | 16.12 | 17.33 | 0.93 |
| | | Mean | 0.96 |
| | | Standard Deviation | 0.03 |

## V. Parametric Study

An extensive parametric study using the finite element model described earlier is conducted. The effect of using many shapes of stiffeners is illustrated by comparing each case involving presence of stiffener with another without a stiffener (unstiffened). Also, the effect of inserting the hole beam or part of it, such as the flanges or the web, through the column. The column used is square hollow section 250x250x10 mm with total height 1500 mm. The steel beam used is IPE 300 connected at the mid-height of the column from one side with length 1500 mm, as shown in Fig. 12. The columns cross sections are chosen to cover the compactness limits according to AISC [20], in which for square column width-to-thickness ratio shall be less than $[1.12\frac{\sqrt{E}}{\sqrt{F_y}}]$, where $F_y$ is the steel yield stress in (t/cm$^2$).

The connection stiffening methods of seven beam column joints were modelled; all beam column joints had the same cross section dimension, with the only difference being the connection stiffening ways, as illustrated in Figs. 13 to 19.

International Journal of Scientific Engineering and Science
Volume 6, Issue 2, pp. 94-106, 2022. ISSN (Online): 2456-7361

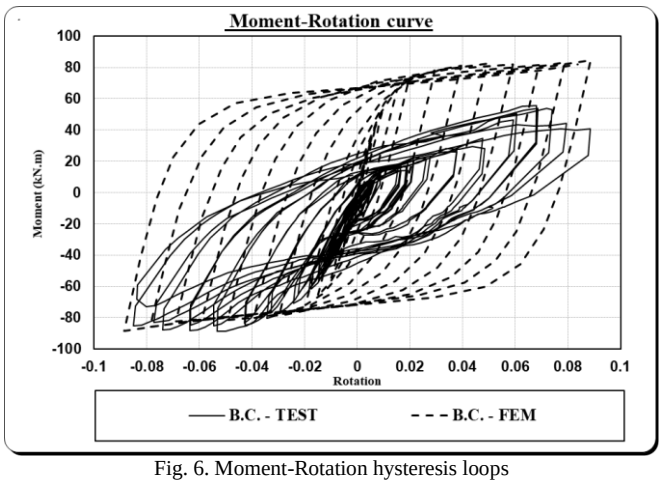


Fig. 6. Moment-Rotation hysteresis loops

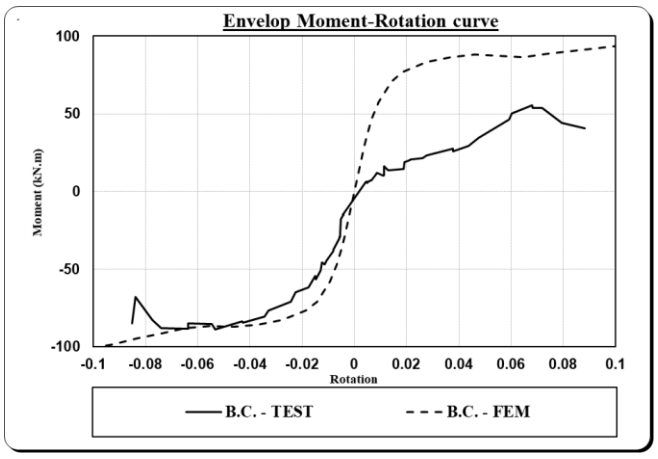


Fig. 7. Envelop Moment-Rotation curve

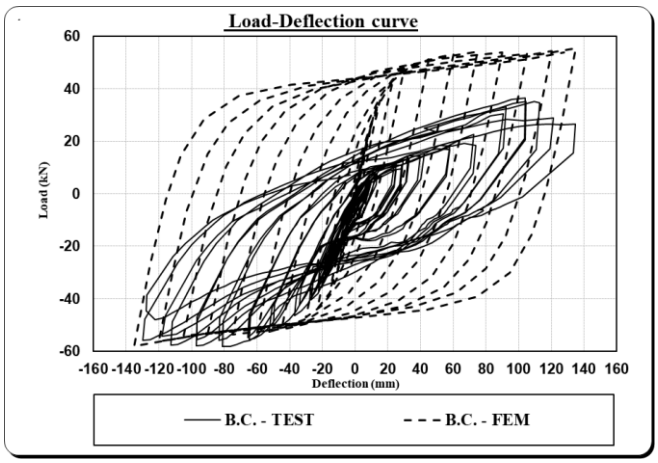


Fig. 8. Load-Deflection hysteresis loops

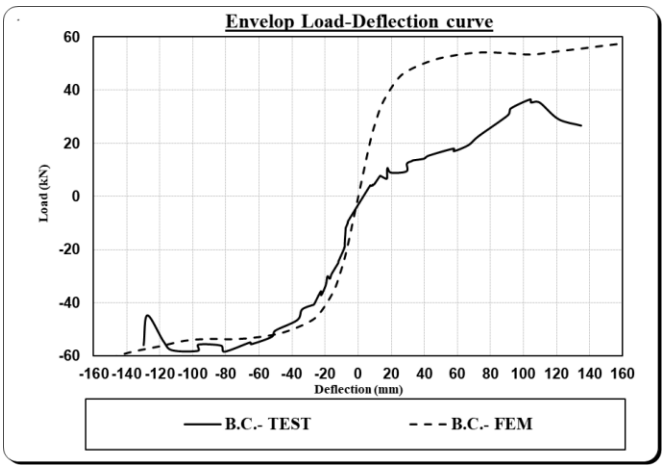


Fig. 9. Envelop Load-Deflection curve

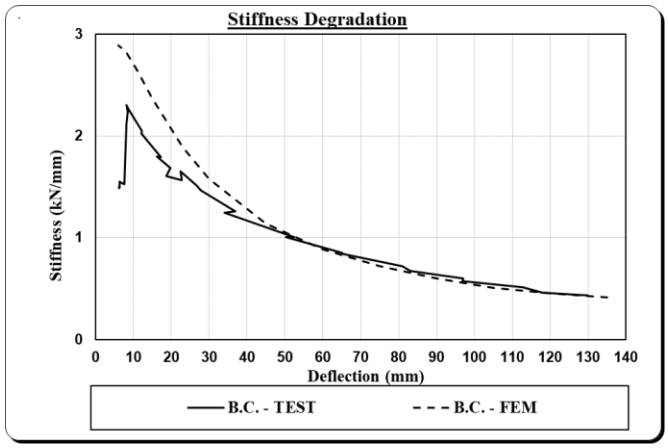


Fig. 10. Stiffness Degradation curve

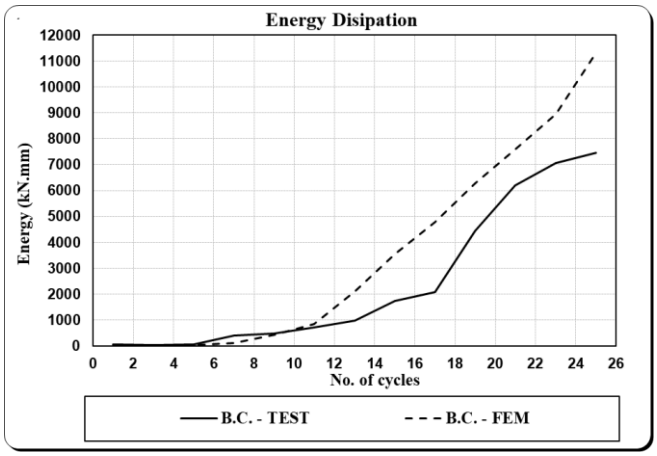


Fig. 11. Energy Dissipation curve

International Journal of Scientific Engineering and Science
Volume 6, Issue 2, pp. 94-106, 2022. ISSN (Online): 2456-7361

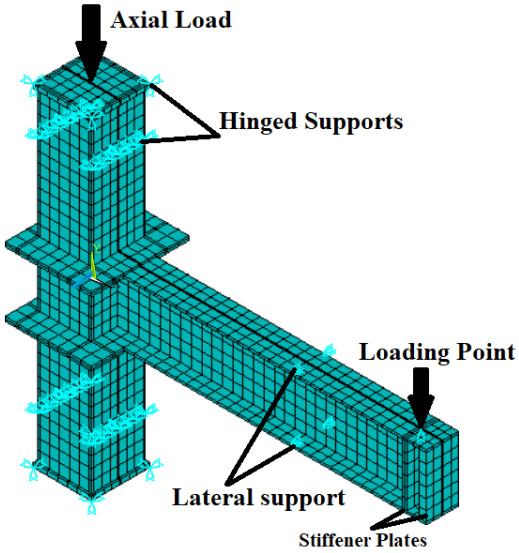

Fig. 12. Finite element model

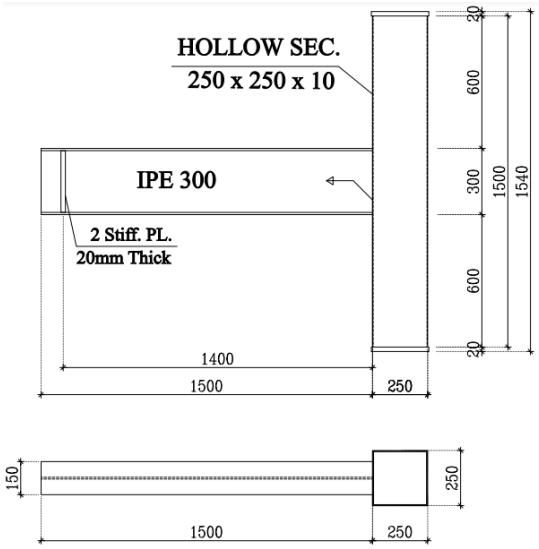

Fig. 13. B.C. without stiffeners (S-1)

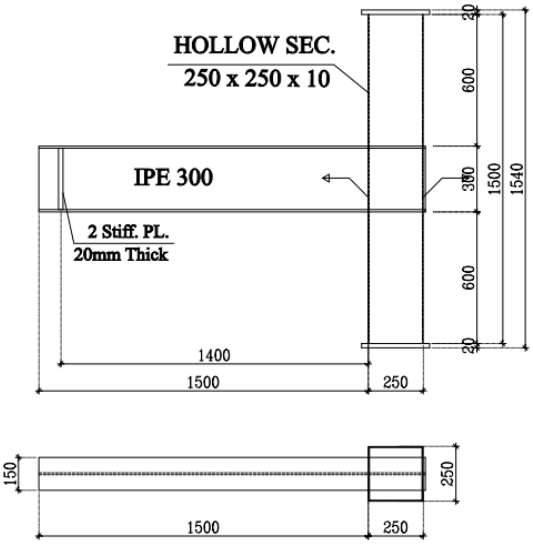

Fig. 14. B.C. beam through column (S-2)

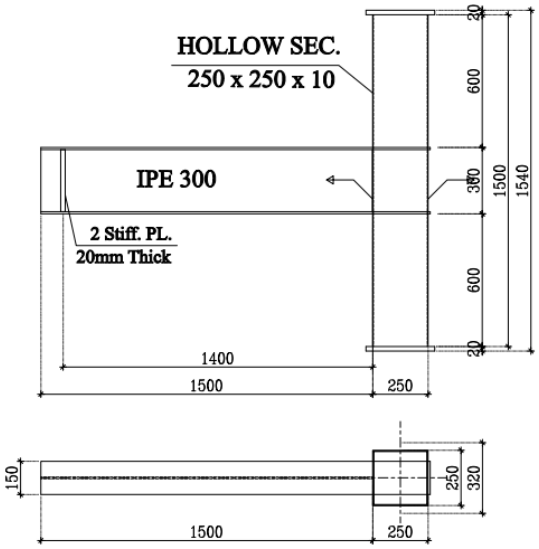

Fig. 15. B.C. beam flange through column (S-3)

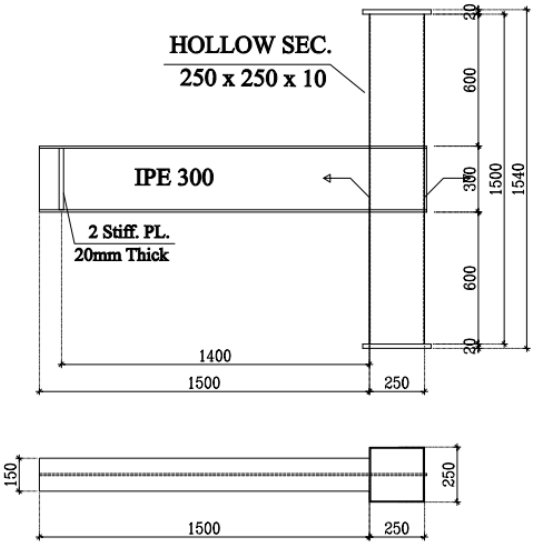

Fig. 16. B.C. beam web through column (S-4)

International Journal of Scientific Engineering and Science
Volume 6, Issue 2, pp. 94-106, 2022. ISSN (Online): 2456-7361

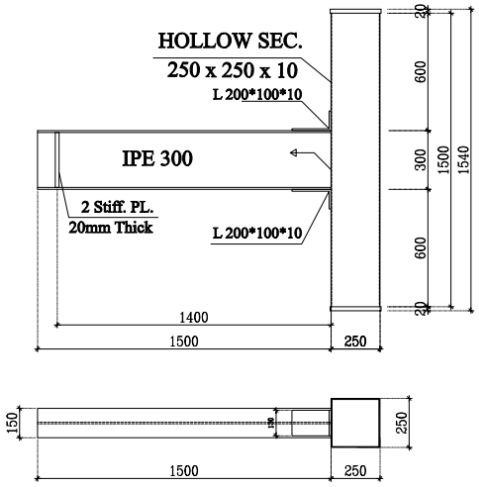


Fig. 17. B.C. Stiffened with Angles (S-5)

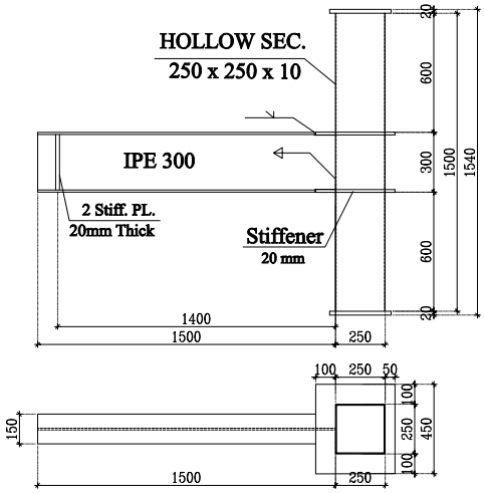


Fig. 18. B.C. Stiffened Plate around the column (S-6)

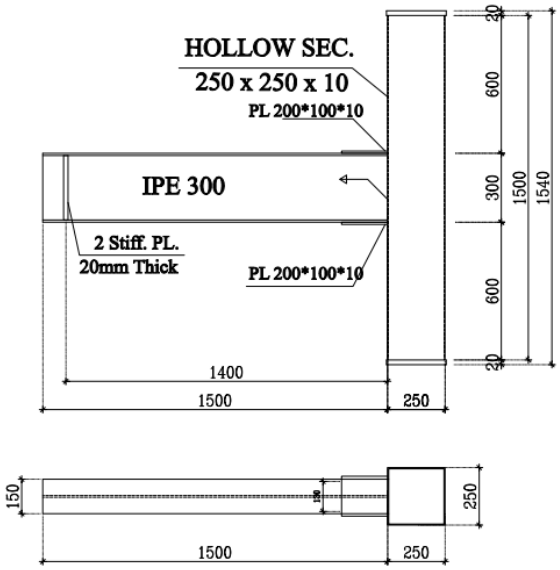


Fig. 19. B.C. Stiffened Plate welded on beam flange (S-7)

## VI. Results and Discussions

The results of the parametric study obtained are represented in the form of tables and curves. The data is put in such a way to give better understanding of the behaviour of beam-to-tubular column connections. A ratio between ultimate moment of the connection and the plastic moment of the beam cross section ($M_{ult}/M_p$) is used in the figures. Each beam column joint's results were documented and will be published separately. All aspects to evaluate include failure mode, cumulative energy, envelope, stiffness deterioration, load-beam displacement hysteresis loops, and connections stresses.

Tables 3 and 4 show the effect of stiffening configurations and types of connection between beam and column on the ultimate moment of the connection between beam IPE 300 and square column (250x10).

### *6.1. Deformed shapes*

Figs. 20 and 21 shows the deformed shape during test for all models. The presence of stiffener angles or plates welded on the beam flanges has no effect on the failure mode as well as the beam flange or web through the column, where the failure occurs at column face, except for specimen's beam column with stiffener plate or beam through column, the models fail at the beam compression flange due to local buckling.

When the columns are unstiffened, high distortion occurs in the steel column wall in which the failure occurs, as shown in Fig. 20. Meanwhile, when the column is stiffened, two different failure modes occur either at stiffener or at compression beam flange regardless of the type of stiffening and connection because the maximum stresses are shifted away from the column, as shown in Fig. 21, where the failure occurs at the beam compression flanges, when inserting the hole beam through the column and the beam column stiffened with plate around the column., local buckling of the beam compression flange occurs. Also, failure of the connection is observed locally at the beam compression flange for columns that are stiffened with stiffener plate around the column and beam through the column except for stiffening with angles or plates on the beam flanges or inserting only the beam flanges or web through the column, failure of the connection is observed at the column face.

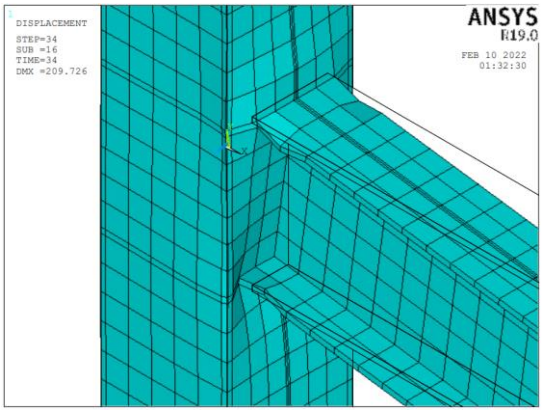


(a) B.C. without stiffeners (S-1)

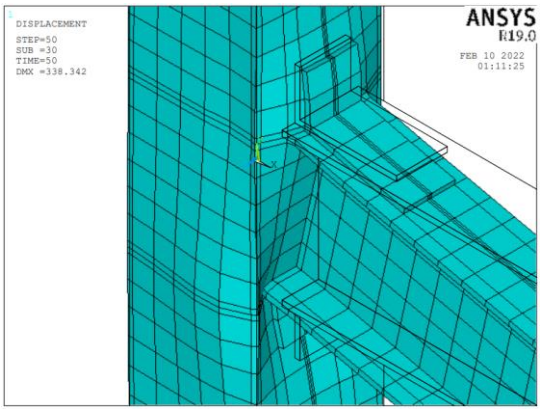


(b) B.C. Stiffened with Angles (S-5)

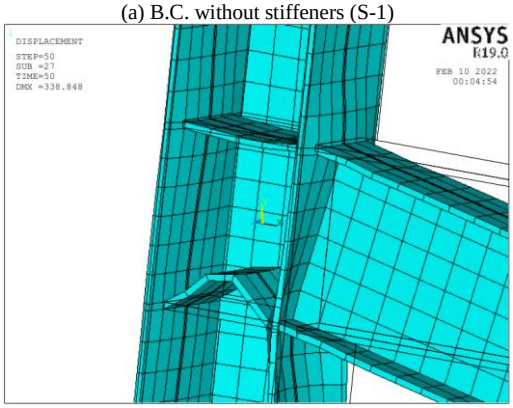


(c) B.C. beam flange through column (S-3)

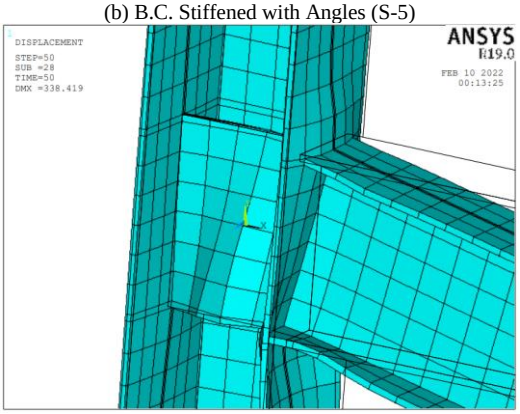


(d) B.C. beam web through column (S-4)

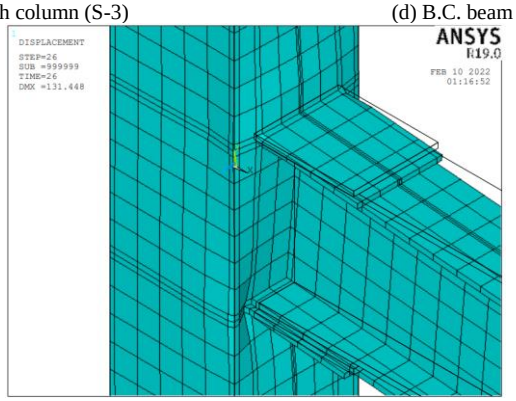


(e) B.C. Stiffened Plate welded on beam flange (S-7)

Fig. 20. (a) to (e) Failure occurs at the column steel wall

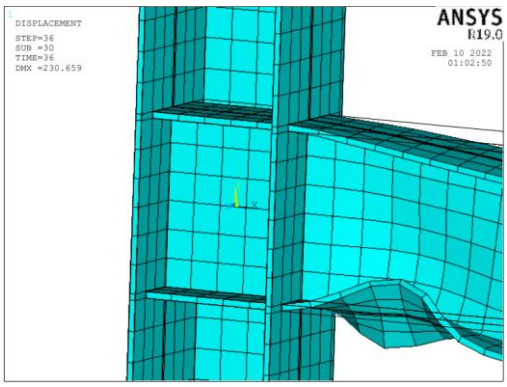


(a) B.C. beam through column (S-2)

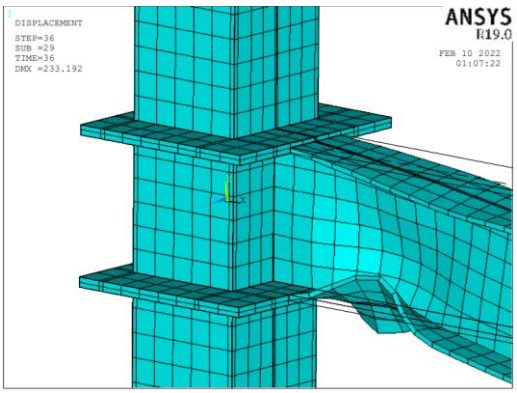


(b) B.C. Stiffened Plate around the column (S-6)

Fig. 21. (a)&(b) Failure occurs at the comp. beam flanges

IJSES
Volume 6, Issue 2, pp. 94-106, 2022.
International Journal of Scientific Engineering and Science
ISSN (Online): 2456-7361

*6.2. Load Deflection Response*

The measured loads were plotted against the applied beam tip displacements at various levels of loading. Fig. 22 depicts the envelop analytical load-deflection for specimens. The analysis of this curve reveals that the beam-column joint's behaviour was initially elastic until a certain point, after which it became plastic. As demonstrated in Fig. 22, the unstiffened beam column had the least capacity and transformed into a plastic condition earlier than the other specimens. This was due to the fact that the tensile force of the beam flange was exclusively carried by the steel tube. Stiffening the beam column joint improves the efficiency of the joint and increases its load capacity from 54.12 kN to 162.7 kN.

Table 3 shows the main test results for the specimens. They illustrate the maximum load and displacement that each specimen can withstand, as well as the ultimate moment, where the maximum load recorded is 162.7 kN for the beam column stiffened with plate around the column (S-6), on the other hand the beam column stiffened with double angles record the maximum displacement with value equal to 195 mm.

The B.C. Stiffened with Angles specimen, as well as the hole beam through the column had almost the same displacement with value 195 mm and 180 mm, respectively. The B.C. stiffened with plate around the column was almost similar to the B.C. with beam through column in both capacity and behavior. The B.C. with flanges or web through column showed a decrease in capacity due to the buckling deformation of the beam flanges or beam web, as shown in Fig.20 (c) and (d).

TABLE 3. The major test results of the specimens

| Model | Sample (Id) | Ultimate level (max. recorded load level) | |
|---|---|---|---|
| | | P (kN) | Δ (mm) |
| **B.C. without stiffeners** | S-1 | 54.12 | 105 |
| **B.C. beam through column** | S-2 | 152.4 | 180 |
| **B.C. beam flange through column** | S-3 | 123.55 | 135 |
| **B.C. beam web through column** | S-4 | 105.46 | 105 |
| **B.C. Stiffened with Angles** | S-5 | 76.72 | 195 |
| **B.C. Stiffened Plate around the column** | S-6 | 162.69 | 135 |
| **B.C. Stiffened Plate welded on beam flange** | S-7 | 67.9 | 120 |

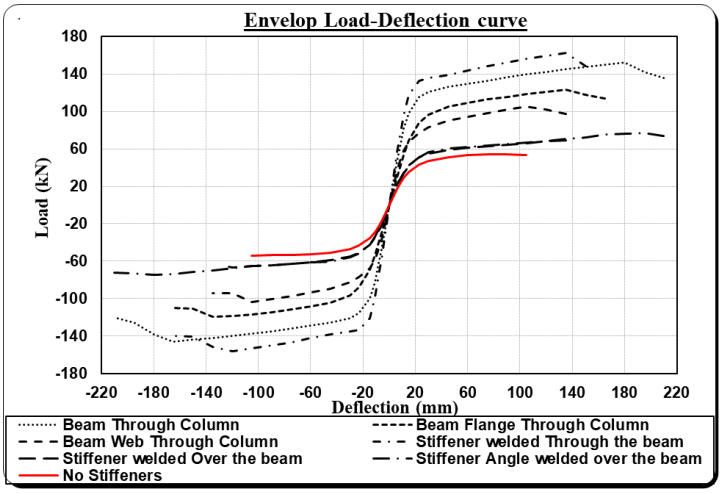


Fig. 22. Envelop Load-Deflection curve

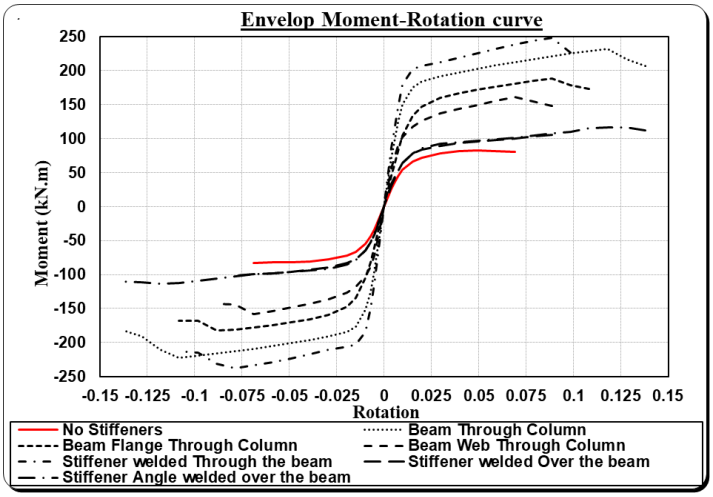


Fig. 23. Envelop Moment-Rotation curve

*6.3. Plastic deformation capacity*

The ability of plastic deformation to absorb huge amounts of energy and shear strain during an earthquake is important to the structure's beam-to-column connection's stability. Members of the seismic force-resisting system (SFRS) that are expected to undergo inelastic deformation have been divided into two categories: moderately ductile and extremely ductile.

According to the AISC Seismic Provisions for Structural Steel Buildings, moderately ductile members are expected to undergo moderate plastic rotation of 0.02 rad or less during the design earthquake, whereas highly ductile members are expected to withstand significant plastic rotation of 0.04 rad or more.

Fig. 23 presents the rotation angle of each specimen under tension in the top and the bottom, all specimens exhibited an inelastic rotation angle of more than 0.02 rad and could be classified as a composite intermediate moment frame, in addition to considering the samples composite special moment frame in addition to high ductile members because the inelastic rotation angle values exceeded 0.04 and could be classified as a composite special moment frame in addition to high ductile members. The inelastic rotation angle of the B.C. with beam through column was the greatest. It is thought that this was because the deformation of the B.C. with beam through column continued on without a brittle failure and with an increase in capacity, after yielding earlier than other specimens. All specimens satisfied the requirements for the composite ordinary moment frame in any case.

*6.4. Ultimate and plastic moment capacity*

Table 4 show the ultimate moment of each model, $M_{ult}$. This table also demonstrate the effect of stiffen the beam-column connection. When the beam column is stiffened with angles (S-5) or plates (S-7) welded over the beam flanges, the ultimate

International Journal of Scientific Engineering and Science
Volume 6, Issue 2, pp. 94-106, 2022. ISSN (Online): 2456-7361

moment increases by (25-40) %, (120 -130) % in the models that use the beam web (S-4) or flanges (S-5) through the column, but the ultimate moment increases by 180 percent and 200 percent when the whole beam is extended through the column and when the beam column stiffened with plate around the column.

Fig. 24 shows that the maximum moment value for every model is smaller than the plastic moment ($M_P$) value of the IPE 300 because of failure, whether as a result of buckling the beam flanges or column, on the other hand, all the stiffened samples reached the values of Plastic rotation ($\theta_P$).

TABLE 4. Ultimate strength of moment connection for Unstiffened Column and stiffened Columns with different stiffener types

| Model (Id) | S-1 | S-2 | S-3 | S-4 | Effect of stiffening Beam Column Connection | | |
|---|---|---|---|---|---|---|---|
| Ultimate Moment value | $M_{ult1}$ (kN.m) | $M_{ult2}$ (kN.m) | $M_{ult3}$ (kN.m) | $M_{ult4}$ (kN.m) | $M_{ult2}/M_{ult1}$ | $M_{ult3}/M_{ult1}$ | $M_{ult4}/M_{ult1}$ |
| | 82.5 | 232.4 | 188.4 | 180.8 | 2.8 | 2.3 | 2.2 |

| Model (Id) | S-1 | S-5 | S-6 | S-7 | Effect of stiffening Beam Column Connection | | |
|---|---|---|---|---|---|---|---|
| Ultimate Moment value | $M_{ult1}$ (kN.m) | $M_{ult5}$ (kN.m) | $M_{ult6}$ (kN.m) | $M_{ult7}$ (kN.m) | $M_{ult5}/M_{ult1}$ | $M_{ult6}/M_{ult1}$ | $M_{ult7}/M_{ult1}$ |
| | 82.5 | 117 | 248.1 | 103.5 | 1.4 | 3 | 1.25 |

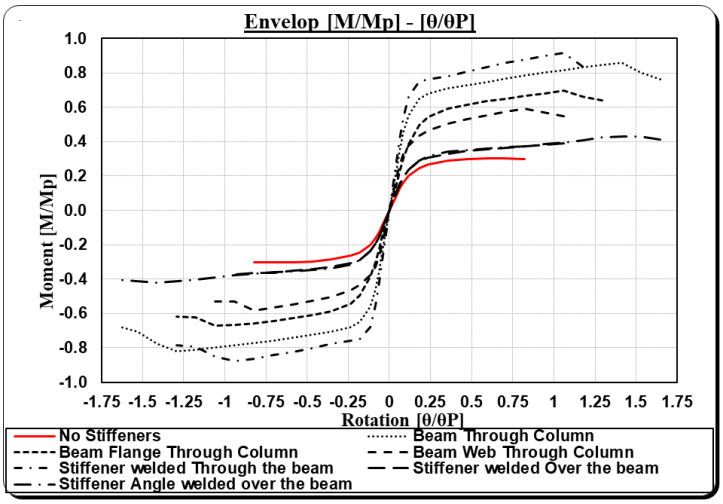


Fig. 24. Envelop [$M/M_P$] - [$\theta/\theta_P$] curve

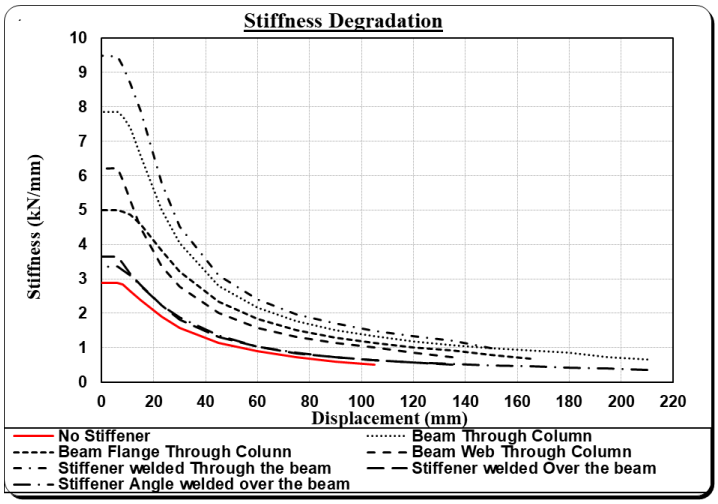


Fig. 25. Stiffness Degradation curve

*6.5. Stiffness Degradation*

Fig. 25. shows the relation between the stiffness degradation versus displacement at each cycle which refers to the displacement level for all specimens. The initial stiffness of all specimens recorded max. values, where before failure, a linear elastic behavior was observed up till the first deformation. The stiffness of the specimen decreased as increased the loading. The initial stiffness of the B.C. stiffened with angles and B.C. stiffened with plate welded over the beam flanges was almost equal, where 30% higher than the unstiffened B.C., for the models with beam web or beam flanges through the column the ratio increased to 80% and 120%, respectively. Stiffening the B.C. by using hole the beam through the column or stiffen plate around the column increase the initial stiffens by 180% and 240%, respectively. Fig. 25 shows the fact that the drop-off in capacity of all models occurred at displacement value equal to (8-12) mm.

*6.6. Stresses*

Figs. 26 to 32 shows maximum von Mises stress values recorded at displacement 255 mm for every model. The common feature in strain values is that the relationship is directly proportional to failure. Stiffening the Beam-column using angles or plate welded over the beam flanges decreases the stress recorded at column face and beam flanges by 18 to 27% and 29 to 31% respectively. Also stiffening the connection with plate around the column decreases the stresses at column face of all specimens by 141%. Likewise, the stress values of the beam flanges for models B.C. stiffened with angles or plates welded over the beam flanges decrease by 15% and 10% respectively, as stiffener angles or stiffener plates decreases the local buckling of the adjacent elements. On the other hand, a stress value of 350 MPa was recorded for the beam immediately after the stiffener for model stiffened with plate around the column, which is 180 % higher than the value recorded at the face of the column. In contrast, for the samples in which the whole beam or beam flanges connected through the column, the max. stress values of the beam flanges recorded increase by 125% and 103% respectively, this shows that the continuity of the beam through the column increases the buckling of the beam flange and thus leads to concentrate and increase stresses more than the direct connection with the face of the column.

International Journal of Scientific Engineering and Science
Volume 6, Issue 2, pp. 94-106, 2022. ISSN (Online): 2456-7361

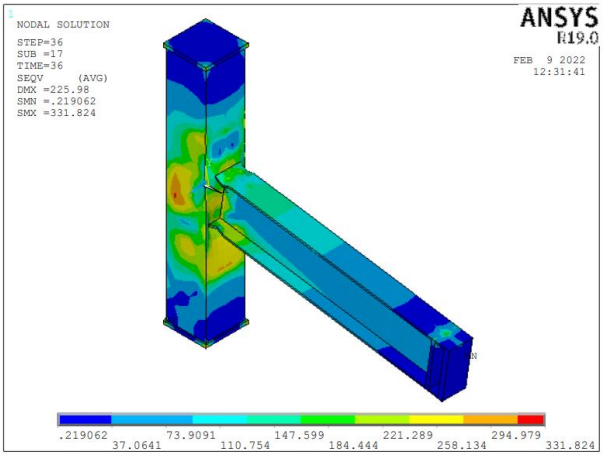


Load = 54.12 kN

Fig. 26. Von Mises stress distribution (N/mm$^2$) of B.C. without stiffeners (S-1)

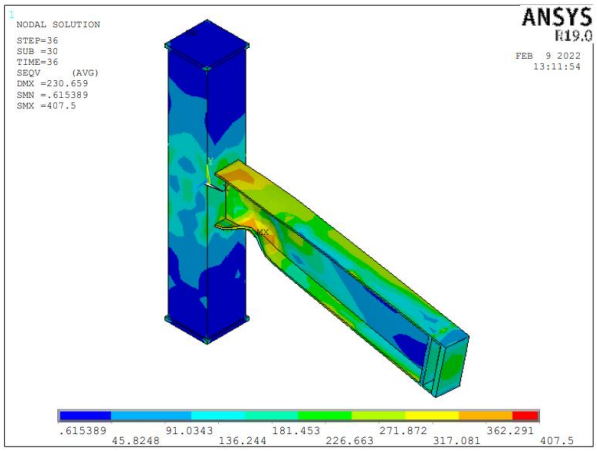


Load = 152.4 kN

Fig. 27. Von Mises stress distribution (N/mm$^2$) of B.C. beam through column (S-2)

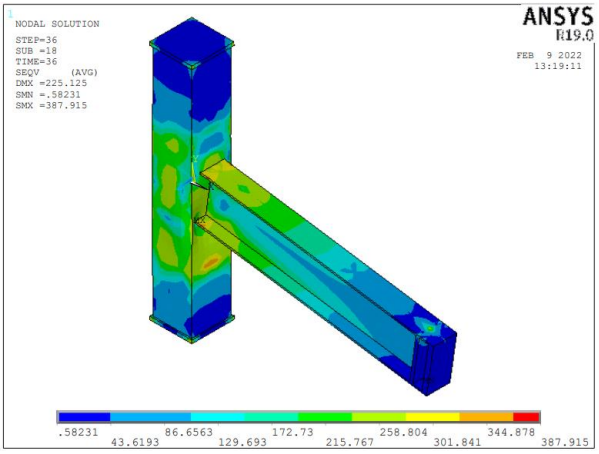


Load = 123.55 kN

Fig. 28. Von Mises stress distribution (N/mm$^2$) of B.C. beam flange through column (S-3)

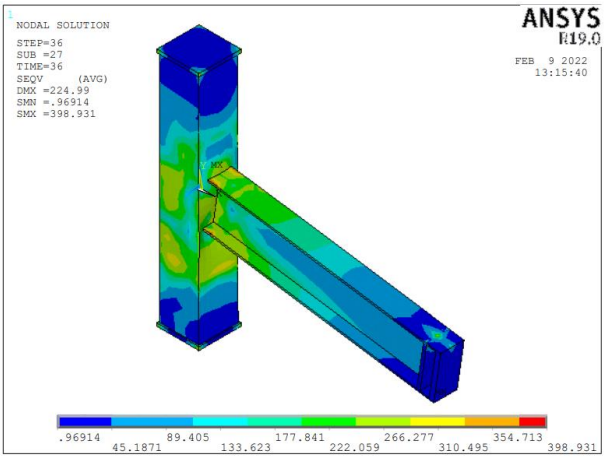


Load = 105.46 kN

Fig. 29. Von Mises stress distribution (N/mm$^2$) of B.C. beam web through column (S-4)

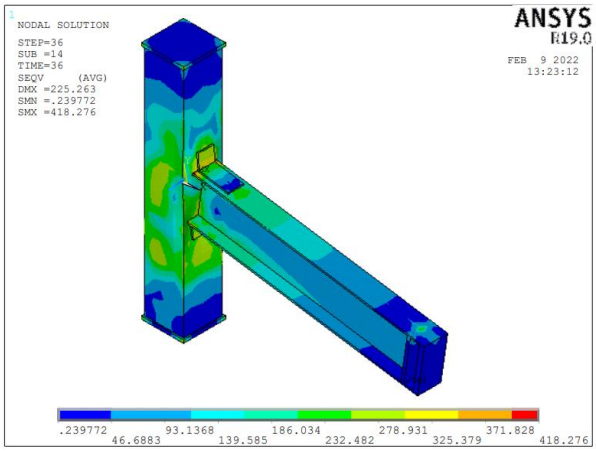


Load = 76.80 kN

Fig. 30. Von Mises stress distribution (N/mm$^2$) of B.C. Stiffened with Angles (S-5)

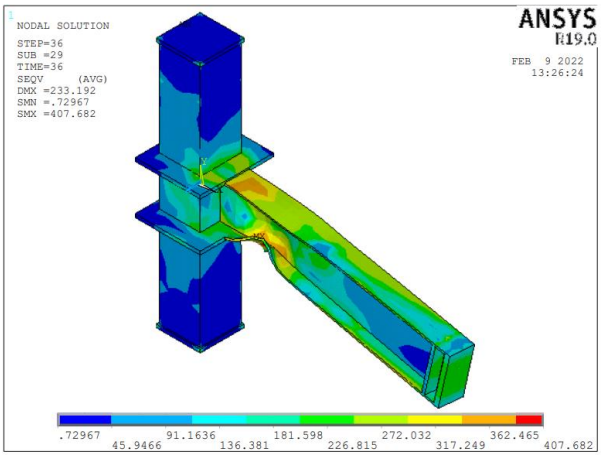


Load = 162.71 kN

Fig. 31. Von Mises stress distribution (N/mm$^2$) of B.C. Stiffened Plate around the column (S-6)

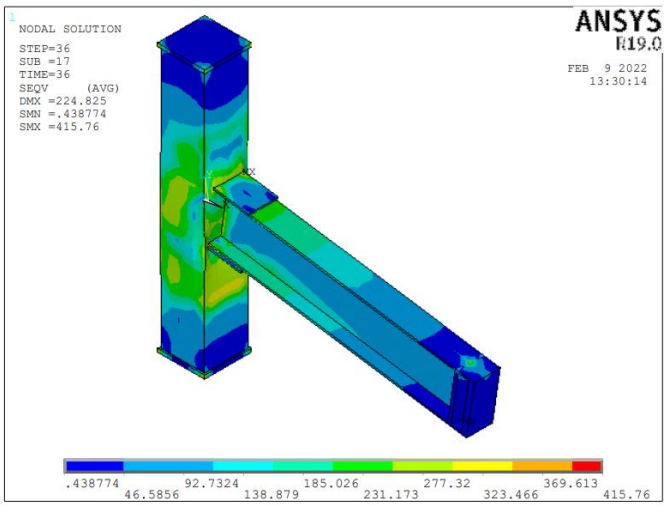


Load = 67.9 kN

Fig. 32. Von Mises stress distribution (N/mm$^2$) of B.C. Stiffened Plate welded on beam flange (S-7)

## VII. CONCLUSIONS

An experimental test was carried out and loaded cyclically. The test specimen is beam to square tube column without stiffener. Analytical study was performed using ANSYS program to predict the ultimate moment of connection between steel I-beams and square tube columns. A parametric study was conducted on six models with different types of stiffening like plates around the column cross sections, angles or plate welded over the beam flanges and inserting the hole beam or only beam flanges or beam web through the column. The study used a cyclic loading test on these connections. The main conclusions obtained from this research are drawn based on the experimental and analytical studies:

1. Stiffening the beam-column connection with plate around the column increases the ultimate moment of the connection by 200% more than the unstiffened column.
2. The results of stiffened connections showed that the ultimate capacities were increased by 25 % for B.C. with plates welded over the beam flanges, 40 % for B.C. with angles and (120-130) % for the B.C. with web or flanges through the column, respectively.
3. Inserting the whole beam through the column increases the ultimate moment by 180%.
4. The B.C. stiffened with plate around the column was almost similar to the B.C. with beam through column in both capacity and behavior.
5. The B.C. with flanges or web through column showed a decrease in capacity due to the buckling deformation of the beam flanges or beam web at the zone inside the tube column.
6. Because both the flanges and the web act as a support for each other, the B.C. with hole beam through column has no buckling or deformation in the flanges or web inside the tube column.
7. Steel column wall failure for un-stiffened columns, as well as stiffener or beam compression flange failure for stiffened columns, three failure modes are observed in the connections. The connection's ductility is greater when the tubes are not stiffened and when use the stiffener as a plates or angles welded over the beam flanges, but the ultimate moment is reduced.
8. The initial stiffness of B.C. stiffened with plate around the column was the highest, where the B.C. stiffened with angles or plate welded over the beam flanges was the minimum with ratio 39 % from the max. stiffness.
9. The drop-off in stiffness capacity of all models occurred at displacement value equal to (8-12) mm, because the connection reaching the yield stress and plastic hinge created.
10. As the cyclic load test results demonstrate, all stiffened connections showed an improvement of ultimate capacity and exhibited an inelastic rotation angle of more than 0.02 rad and could be classified as a composite intermediate moment frame. The models had an inelastic rotation angle of more than 0.03 rad and could be classified as a composite special moment frame in addition to high ductile members.

These cyclic load results demonstrated that the suggested connection types, could obtain more than 0.01 rad of the inelastic rotation capacity, and so could be classified as a composite ordinary moment frame and have sufficient seismic performance. Therefore, it is concluded that the beam to tube column connections can be safely used in weak earthquake regions.

## REFERENCES

[1] Kim, Y. J., & Oh, S. H. (2007). Effect of the moment transfer efficiency of a beam web on deformation capacity at box column-to-H beam connections. Journal of Constructional Steel Research, 64, 24–36.

[2] Saneei Nia, Z., Ghassemieh, M., & Mazroi, A. (2013). WUF-W connection performance to box column subjected to uniaxial and biaxial loading. Journal of Constructional Steel Research, 88, 90–108.

[3] Saneei Nia, Z., Ghassemieh, M., & Mazroi, A. (2014a). Panel zone evaluation of direct connection to box column subjected to bidirectional loading. The Structural Design of Tall and Special Building, 23, 833–853.

[4] Saneei Nia, Z., Mazroi, A., Ghassemieh, M., & Pezeshki, H. (2014b). Seismic performance and comparison of three different I beam to box

column joints. Earthquake Engineering and Engineering Vibration, 13(4), 717–729.
[5] Saneei Nia, Z., Mazroi, A., & Ghassemieh, M. (2014c). Cyclic performance of flange-plate connection to box column with finger shaped plate. Journal of Constructional Steel Research, 101, 207–223.
[6] Song, Q. Y., Heidarpour, A., Zhao, X. L., & Han, L. H. (2015). Performance of unstiffened welded steel I-beam to hollow tubular column connections under seismic loading. International Journal of Structural Stability and Dynamics, 15(1), 14500331–145003323.
[7] Song, Q. Y., Heidarpour, A., Zhao, X. L., & Han, L. H. (2016). Performance of double-angle bolted steel I-beam to hollow square column connections under static and cyclic loadings. International Journal of Structural Stability and Dynamics, 16(2), 14500981–145009820.
[8] Ehab Ellobody and Ben Young, "Nonlinear analysis of concrete-filled steel SHS and RHS columns", *Thin-Walled Structures*, 44, 919-930, (2006).
[9] Georgios Giakoumelis and Dennis Lam, "Axial capacity of circular concrete-filled tube columns", *J. Construction Steel Research*, 60, 1049-1068, (2004).
[10] Johansson, M., and Gylltoft, K, "Mechanical behavior of circular steel-concrete composite stub columns" J. Structural Engineering, ASCE, 128(8), 1073–1081, (2002).
[11] Kyung-Jae Shin, Young-Ju Kim, Young-Suk Oh, and Tae-SupMoon, "Behavior of welded CFT column to H-beam connections with external stiffeners", *Engineering Structures*, 26, 1877-1887, (2004).
[12] Toshiyuki Fukumoto, "Steel beam to concrete-filled steel tube column, moment connections in Japan", Steel Structures, 5, 357-365, (2005).
[13] Ying Wang, Yuan Xuan and Pengfei Mao, "Nonlinear finite element analysis of the steel-concrete composite beam to concrete-filled steel tubular column joints", International Journal of Nonlinear Science, 9, No. 3, 341-348, (2010).
[14] Young-Ju Kim, Kyung-Jae Shin and Wha-Jung Kim, "Effect of stiffener details on behavior of CFT column-to-beam connections", Steel Structures, 8, 119-133, (2008).
[15] Yousef M. Alostaz, and Stephen P. Schneider, "Connections to concrete-filled steel", Report, Department of Civil Engineering, University of Illinois, Urbana, Champaign, (1996).
[16] ANSYS, finite element program, Swanson Analysis System, Inc., Release 12.1, (2009).
[17] ANSI/AISC 360-10. Specification for structural steel buildings. American Institute of Steel Construction, Chicago; 2010.
[18] American Institute of Steel Construction. Inc. AISC. Supplement 1 and 2 to seismic provisions for structural steel buildings. Chicago (IL): AISC. May 21; 2002.
[19] ANSYS, finite element program, Swanson Analysis System Inc., Release 12.1, (2009).
[20] ANSI/AISC 360-10. Specification for structural steel buildings. American Institute of Steel Construction, Chicago; 2010.